Journal of Industrial and Engineering Chemistry 91 (2020) 347–354

Contents lists available at ScienceDirect

Journal of Industrial and Engineering Chemistry

journal homepage: www.elsevier.com/locate/jiec

The effect of viscosity ratio on drop pinch-off dynamics in two-fluid flow

Xiaofeng Jiang[a,b], Enle Xu[a], Xianliang Meng[a], Huai Z. Li[b,*]

[a] School of Chemical Engineering and Technology, China University of Mining and Technology, Xuzhou 221116, PR China
[b] Laboratory of Reactions and Process Engineering, CNRS, University of Lorraine, 1, Rue Grandville, BP 20451, 54001 Nancy Cedex, France

ARTICLE INFO

Article history:
Received 16 June 2020
Received in revised form 1 August 2020
Accepted 14 August 2020
Available online 20 August 2020

Keywords:
Drop
Pinch-Off
Viscosity
Ratio
Self-Similar
Scaling

ABSTRACT

Drop pinch-off draws a lot of interest from scientists and engineers because of widely practical applications as well as the fascinating mechanism of finite-time singularities and self-similar behavior. This work experimentally investigates the effect of viscosity ratio on the local pinch-off mechanism of liquid drops in both air and viscous fluids, with a high-speed camera. The results show that for $56 \leq \lambda \leq 6.3 \times 10^3$ and $0.009 \leq \lambda \leq 0.061$, drop pinch-off exhibits self-similar profile which is asymmetric and conical away from h_{min}. Drop pinch-off in air with low viscosity ratios shows either in inertial regime (I) or transition from inertial to viscous regime (I→V). But the kinetics undergoes the inertial regime (I) to inertial-viscous regime (IV) through an intermediate viscous regime (V) when the viscosity ratio becomes larger. Drop pinch-off in viscous fluids displays the transition from inertial to viscous regime (I→V). These results agree well with Eggers's universal solution until it becomes unstable and the previous literature. The viscosity ratio indeed affects the drop pinch-off dynamics as well as interface deformation. Our experiments enrich the understanding of the interaction between the internal and external fluids on drop pinch-off behavior near the singularity point.

Introduction

Liquid drop formation and breakup dynamics no matter at macroscale [1–3] or at microscale [4–6] attracts a lot of attentions from different disciplines due to their importance in diverse established and cutting-edge technologies, such as ink-jet printing, fiber spinning, spray coating, DNA arraying, emulsification, and atomization. For most applications, the volume of newly drop, frequency of drop formation as well as size distribution of droplets are of great importance and well investigated. However, the research focus has now switched from these gross features to the final and local dynamics. When the minimum diameter of the thread connecting the forming drop and the feeding liquid goes to zero, a space-time singularity point occurs where the dynamical description breaks down and the curvature, velocity and pressure all diverge to infinity. Because of the much smaller length and time scales in the immediate neighborhood of singularity, the dynamics near the singularity point evolve independently of the initial and boundary conditions. Thus, the dynamics near the singularity exhibits self-similarity.

For the rupture of liquid threads surrounded by a dynamically inactive air, Keller and Miksis [7] were the first to propose a scaling theory to describe the self-similar recoil of a liquid sheet upon its rupture. Peregrine et al. [8] were first to suggest that the dynamics near breakup are universal, through the non-linear equations of neck evolution. Since their pioneering work, scaling theories were developed to understand the pinch-off dynamics of liquid threads. For a low viscosity liquid, the initial thinning of liquid thread occurs in inertial regime (I) where inertial and capillary forces balance, and the minimum neck diameter scales with the time-to-pinch-off as $h_{min} \sim \tau^{2/3}$ [9,10]. While for a viscous liquid, the initial thinning of liquid thread occurs in viscous regime (V) where viscous and capillary forces balance, and the minimum neck diameter scales with the time-to-pinch-off as $h_{min} \sim \tau$ [11,12]. When the thread is infinitesimally small, both the viscous force in inertial regime (I) and inertial force in viscous regime (V) takes effect, so that the latter thinning dynamics enters into inertial-viscous regime (IV) where inertia, viscous force and capillary force are all important [13]. Besides the three major scaling theories, several transitory regimes were also demonstrated. The crossover from inertial regime (I) or viscous regime (V) to inertial-viscous regime (IV) was

* Corresponding author.
E-mail address: Huai-Zhi.Li@univ-lorraine.fr (H.Z. Li).

https://doi.org/10.1016/j.jiec.2020.08.019
1226-086X/

confirmed numerically and experimentally by previous researchers [13,14]. These intermediate transitory regimes make the overall picture more complicated and were summarized and developed by Li and Sprittles [15]. However, when the minimum neck diameter reaches a limited value, the dynamics of the out fluid can no longer be neglected.

Drop pinch-off is a two-phase interfacial problem and the viscosity ratio λ plays a great effect on the final pinch-off dynamics. Here, λ is the viscosity ratio between internal and external fluids, $\lambda = \eta_{in} / \eta_{ex}$. η_{in} and η_{ex} are the viscosities of internal and external fluids, respectively. Doshi et al. [16] experimentally and numerically investigated the pinch-off of a water drop in an extremely viscous fluid, $\lambda = 8.3 \times 10^{-5}$. The results showed the pinch-off dynamics exhibits non-self-similarity and non-universality, and the memory of the initial and boundary conditions persists. Lister and Stone [17] numerically investigated the breakup of a viscous thread surrounded by another viscous fluid and indicated that the viscosity of the external fluid modifies the asymptotic structure of capillary breakup near the singularity and the asymptotic balance is between surface tension and viscous stresses in two fluids while inertia is negligible. Pan and Suga [18] used the level-set method to track the interface of liquid jets pinching off in ambient fluids with viscosity ratio of $0.17 \leq \lambda \leq 1.7$. Cohen et al. [19] experimentally and theoretically studied the two-fluid pinch-off problem, focusing on the viscosity effect on drop shape and breaking rate and revealed the self-similar behavior for the range $0.02 \leq \lambda \leq 30$. Zhang and Lister [20] numerically analyzed the capillary instability of a fluid thread in a surround fluid with $1/16 \leq \lambda \leq 16$ and proved the universal similarity scaling is preserved.

Though the previous researchers were dedicated to investigate the pinch-off dynamics either in air or in another fluid, the effect of viscosity ratio on local mechanism and deformation of drop pinch-off has not yet been fully understood. Thus, this experimental work goes further to investigate the two-fluid systems with extended range of viscosity ratio ($56 \leq \lambda \leq 6.3 \times 10^3$ and $0.009 \leq \lambda \leq 0.061$), aiming at gaining some insights into different pinch-off characteristics of liquid drop approaching to the singularity point.

Experimental setup and methodology

A schema of the experiment setup is illustrated in Fig. 1. The stainless steel nozzle I (outside diameter d' =0.97 mm and inner diameter d =0.6 mm) and nozzle II (outside diameter d' =2.5 mm and inner diameter d =1.8 mm) were used to generate liquid drops. The pinch-off behaviors were recorded with a Phantom v7.11 camera (Vision Research, USA) at rates up to 1 000 000 frame per second (fps). A macro lens (MP-E 65 mm f/2.8, Canon, Japan) was coupled with the high-speed camera. For drop-in-air system, the resolutions were mainly 192×400 pixels with 51,012 fps and 304×400 pixels with 39,013 fps for nozzle I and nozzle II, respectively. The pinch-off behavior of silicon oils in air was recorded with larger resolutions depending on the length of the elongated thread. For drop-in-fluid system, the resolution was mainly chosen to be 304×264 pixels, 50,000 fps and 432×480 pixels, 20,000 fps for nozzle I and nozzle II, respectively. A point light source (KL 2500 LED, Schott, Germany) was employed to illuminate the drop. The exposure time was as low as 3 μs with the scale of 4 μm/pixel. A syringe pump (Hamilton, Germany) was adopted to control the flowrate (Q) within the range of (0.01–1.00) mL/min. All images were recorded after the formation process reaching a steady state. The obtained images were analyzed frame by frame through the self-programmed Matlab. Firstly, the images were converted into black-and-white by a preset threshold value and verified with the exact length scale. Secondly, the interested section was selected and the neck diameter counted row by row. Thus, the minimum neck diameter in each image was then obtained. These sequences were completely reproducible. Three pinch-offs were analyzed for each studied set of parameters, and the morphology as well as the thread evolution were repeatable among three pinch-offs.

The initial conditions, such as nozzle diameter, drop size, surface tension and viscosity were studied. To analyze the effect of viscosity ratio on the drop pinch-off, the internal and external fluids were prepared. The internal fluids consisted of various Newtonian fluids: deionized water, emkarox HV 45 (Emkarox) aqueous solution, silicone oil 47 V (silicone oil). Silicone oils were purchased from VWR Chemicals and used depending on their viscosity: silicone oil 47 V10 (SO 10), silicone oil 47 V50 (SO 50) and silicone oil 47 V100 (SO 100) [21–23]. While the external fluids in our experiments were air, silicone oil 50 and silicone oil 100. The physical properties of drop-in-air and drop-in-liquid systems were given in Table 1 and 2, respectively. ρ, σ and η stands for the density, surface tension and viscosity of the liquid. λ is the viscosity ratio between internal and external fluids and l_η is the viscous length, $l_\eta = \eta^2/(\sigma\rho)$. Ohnesorge number ($Oh = \eta/(\rho d\sigma)^{0.5}$), which is the ratio of viscous force to the square root of the product of surface tension and inertial forces, are all smaller than 1, except SO 50 and SO 100 whose *Oh* number is close to 1.

Results and discussion

Drop pinch-off in gas-liquid two phase flow

Fig. 2 shows the sequences of various liquid drops pinch-off in air with different viscosity ratios. For a low viscosity liquid drop, as shown in Fig. 2a-2 c, when the surface tension is surpassed by the inertial force, a liquid thread of minimum diameter h_{min} occurs and rapidly increases in length and decreases in width, which eventually bifurcates into the upper and bottom ends connecting by the conical thread. The thread loses its uniformity and

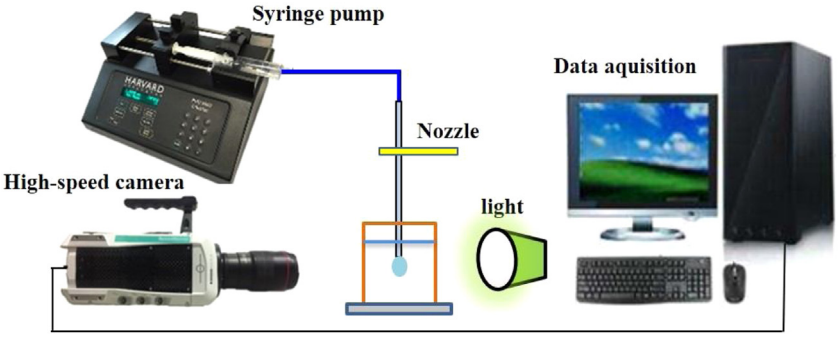

Fig. 1. Scheme of the experimental setup. The tank (made of PMMA with inside three dimensions: $5 \times 5 \times 6.5$ cm) was filled with silicone oil for drop-in-fluid system. While for drop-in-air system, the liquid tank was just removed.

Table 1
Fluid properties of drop-in-air system at 20 °C [21].

Drop-in-air system	ρ/(kg/m^3)	σ/(mN/m)	η/(mPa.s)	$\lambda = \eta/\eta_{air}$	$l_\eta = \eta^2/(\sigma\rho)$
Water	996	72.50	1.0	56	13.85 nm
0.50 wt% Emkarox + water	996	70.00	2.0	1.1×10^2	57.37 nm
4.50 wt% Emkarox + water	998	68.00	3.6	2.0×10^2	190.97 nm
Silicone oil 10 (SO 10)	920	19.70	11.5	6.4×10^2	7.30 μm
Silicone oil 50 (SO 50)	955	20.10	59.5	3.3×10^3	184.43 μm
Silicone oil 100 (SO 100)	960	20.20	112.8	6.3×10^3	656.14 μm

*The external fluid is air with density 1.29 kg/m^3 and viscosity 0.018 mPa.s.

Table 2
Fluid properties of drop-in-fluid system at 20 °C [22].

Drop-in-liquid system	In SO 50		In SO 100	
	σ/(mN/m)	$\lambda=\eta/\eta_1$	σ/(mN/m)	$\lambda=\eta/\eta_2$
Water	20.20	0.017	17.60	0.009
0.50 wt% Emkarox + water	20.10	0.034	17.70	0.018
4.50 wt% Emkarox + water	19.70	0.061	17.50	0.032

*The subscript (1) and (2) stand for external fluids SO 50 and SO 100, respectively.

continuously elongates until a critical length where it pinches off first at the bottom and then at the upper end. For a slightly high viscosity fluid: SO 10 ($\lambda = 6.4 \times 10^2$), as shown in Fig. 2d, a long thread connects the two ends and becomes thinner and thinner. In the very vicinity of pinch-off point, the bottom end of the long thread evolves into a micro-thread, as shown in the enlarged image at τ = -0.03 ms in Fig. 2d. During the next tens of microseconds, the micro-thread detaches from the bottom and a newly drop forms. The micro-thread rebounds into the primary thread in a few microseconds, and the upper end of the thread extracts another micro-thread, as shown in the enlarged image at τ =0.23 ms in Fig. 2d. Finally, the thread detaches from the liquid connected by the nozzle. But for the high viscosity fluids of SO 50 ($\lambda = 3.3 \times 10^3$) and SO 100 ($\lambda = 6.3 \times 10^3$) pinch-off in air, as shown in Fig. 2e and 2 f, the liquid thread evolves into a long filament and then pinch off in the way of spinning with several pinch-off points, some bulges and some separate satellite droplets.

It can be observed that the critical length of liquid thread increases with the viscosity ratio due to the viscous resistant opposing the capillary pressure [24]. For low viscosity ratio, both the bottom of the nozzle fluid and the top of the newly-formed drop after two pinch-off points develop into plane surfaces, and the thread evolves into a chain of droplets, as shown in Fig. 2a-2 c, which quickly merge into one large satellite drop. Recoil and interfacial instability produce capillary waves that lead to the chain of droplets and the plane part on the top of the newly drop [25]. For slightly high viscosity ratio in Fig. 2d, the plane surface was also observed at both the bottom and the top of the thread and one large satellite drop formed without the occurrence of a chain of droplets. However, for highly viscous fluids in Fig. 2e and 2 f, both the bottom of the nozzle fluid and the top of the newly drop evolves into smooth curved surface with small tails, as indicated in the blowup. For $56 \leq \lambda \leq 6.4 \times 10^2$, the liquid thread breaks in the form of "end pinch-off" mode with one satellite drop, while for $\lambda = 3.3 \times 10^3$ and $\lambda = 6.3 \times 10^3$, the long filament undergoes several perturbations and ultimately breaks somewhere between these perturbations in the form of "internal-pinching" mode with multiple pinch-off points as well as varying-sized satellite droplets. The stability of liquid thread or filament to perturbations determines the "end pinch-off" or "internal-pinching" [26]. The shape analyses demonstrate the viscosity ratio between internal and external fluids greatly affect the deformation and evolution liquid drop during pinch-off process.

In fact, the internal viscosity is an important factor for drop pinch-off in air at length scale smaller than the viscous length $l_\eta = \eta^2/(\sigma\rho)$ [27,28]. For fluids of low viscosity water and Emkarox aqueous solutions in this work, the viscous length scale l_η (given in Table 1) is typically of order of nanometer, out of the present optical resolution, and thus they can be described as inviscid

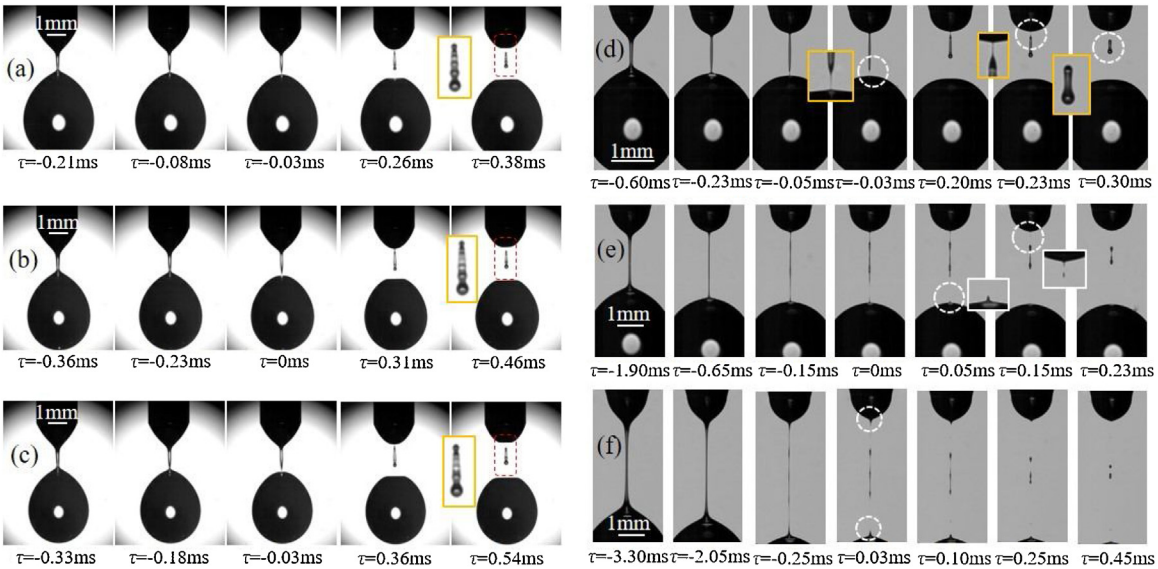

Fig. 2. Pinch-off sequences of different liquids in air. (a) $\lambda = 56$; (b) $\lambda = 1.1 \times 10^2$; (c) $\lambda = 2.0 \times 10^2$; (d) $\lambda = 6.4 \times 10^2$; (e) $\lambda = 3.3 \times 10^3$; (f) $\lambda = 6.3 \times 10^3$. Remaining time τ is donated as the time relative to the first pinch-off point. (a-c) share the same scaling bar.

pinch-off without visible micro-thread. The value of l_η for SO 10 is several micrometers close to the available optical resolution and usually it's called viscous pinch-off with long liquid thread and visible secondary micro-thread. For the much higher viscosity like SO 50 and SO 100, the value of l_η is several hundred micrometers which are close to the order of millimeter, then comparable to the nozzle diameter, resulting in spinning pinch-off with several singularities and many satellite droplets. In reality, once the thread width is smaller than l_η, the viscous stresses gain weight and compete with other forces. Thus, the higher the viscosity ratio, the more the instabilities and the more the satellite droplets.

For Newtonian fluids, the local balance of inertial, viscous and capillary force results in the universal evolution of the liquid thread, and the profiles could be imposed to be self-similar with appropriate scaling [29]. Fig. 3 presents the profile of liquid thread near the first pinch-off point in the form of h/h_{min} *vs.* $(z\text{-}z_{min})/h_{min}$ for λ = 56. Here, h_{min} is the minimum diameter of the thread, $h(z)$ is the thread diameter at position of z, and z_{min} is the axial location of the minimum thread diameter, as denoted in the Fig. 3a. Obviously, the thread profile of water with Q =0.1 mL/min and d =1.8 mm, diverges at larger remaining times while near the pinch-off point, it becomes self-similar. The thread profiles at different nozzle diameters and flowrates at the final pinch-off region are superimposed as shown in Fig. 3a, implying the self-similar profile is independent of initial conditions. The same self-similar evolution of liquid thread was also observed for $\lambda = 6.4 \times 10^2$, as shown in Fig. 3b. Even for the high viscosity ratios $\lambda = 3.3 \times 10^3$ and $\lambda = 6.3 \times 10^3$, the self-similar profile was preserved, which agrees well with the existing literature [30]. Fig. 3c presents the thread profiles of the different viscosity ratios next to the singularity point. The thread profiles of the smaller viscosity ratios of $\lambda = 56$, $\lambda = 1.1 \times 10^2$ and $\lambda = 2.0 \times 10^2$ are almost superimposed while the larger viscosity ratio of $\lambda = 6.4 \times 10^2$ exhibits a different thread evolution. In addition, the liquid thread of $\lambda = 3.3 \times 10^3$ and $\lambda = 6.3 \times 10^3$ exhibits a special evolution and the profile deviates dramatically due to the small tail on the top of the to-be-formed drop. This is possibly due to the fact that the large viscous length scale leads to the increasing weight of viscous force.

In order to quantitatively investigate the pinch-off dynamics, the universal scaling law $h_{min} \propto \tau^b$ was adopted with a dimensionless analysis method. We plot the dimensionless minimum neck diameter h_{min}/d as a function of dimensionless time-to-pinch-off τ/t_{cap} at different λ and l_η in Fig. 4. Here, h_{min} is the minimum neck diameter, d is the nozzle inner diameter, b is the scaling exponent, τ is time to pinch-off, and t_{cap} is the capillary time, $t_{cap} = (\rho d^3/\sigma)^{0.5}$. Fig. 4a shows the evolution of dimensionless minimum neck diameter of water pinch-off in air under different conditions and obviously it could be observed that the memory of the initial conditions like the flowrate and nozzle diameter are lost during the final pinch-off stage. A difference could be observed for exponents in Fig. 4b: for relatively low viscosity ratio ($56 \le \lambda \le 2.0 \times 10^2$), the pinch-offs exhibit a classical exponent of 2/3, corresponding to the inertial regime (I); while the pinch-off of relatively high viscosity ratio ($\lambda = 6.4 \times 10^2$) shows an exponent of 2/3 firstly and then 1, corresponding to the inertial regime (I) and viscous regime (V) respectively. Ohnesorge number for $56 \le \lambda \le 6.4 \times 10^2$ are quite smaller than 1, so the inertial regime (I) occurs first and the inertial-viscous regime (IV) couldn't be attained due to the optical limitation for smaller length and time scale [13]. Fig. 4c shows the evolution of dimensionless minimum neck diameter of SO 10, SO 50 and SO 100 pinch-off in air. Apparently, the dimensionless minimum neck diameter diverges from each other, and the larger viscosity ratio leads to a slower thinning kinetics. This is due to the fact that the internal fluid with higher viscosity results in a long filament and thins more slowly [27]. The route

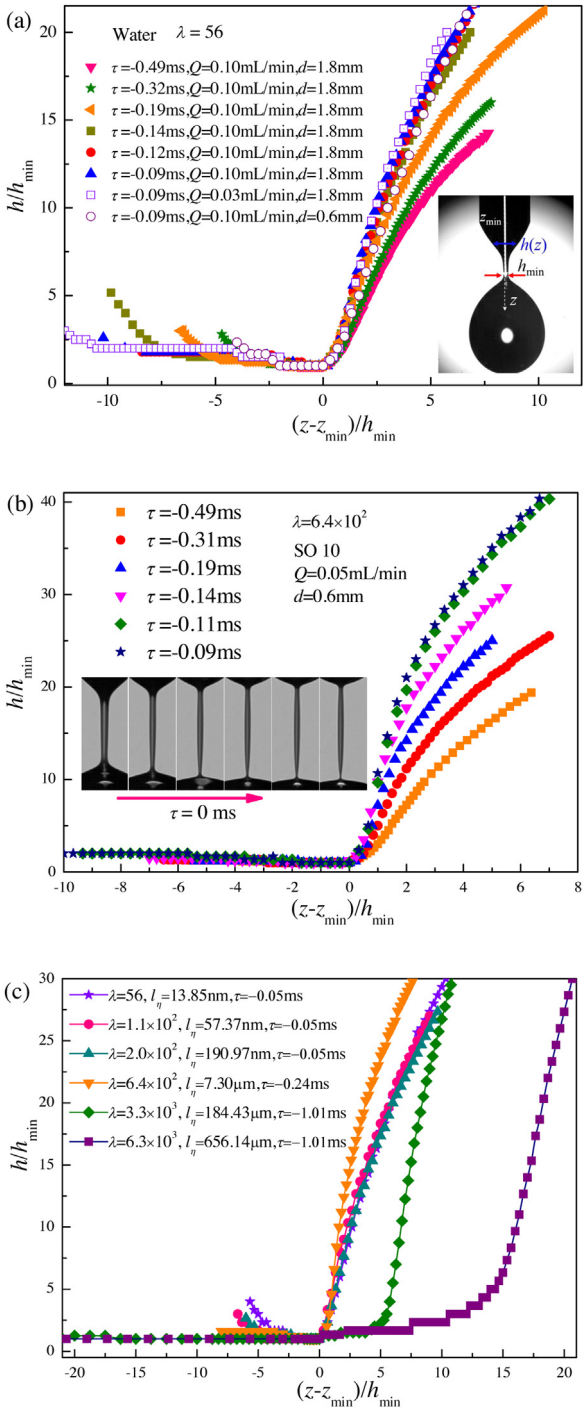

Fig. 3. Profiles of liquid thread in the very vicinity of first pinch-off point. (a) water pinch-off in air with λ = 56; (b) SO 10 drop pinch-off in air with $\lambda = 6.4 \times 10^2$; (c) drop pinch-off with different viscosity ratios in the vicinity of pinch-off point. Due to the beads-on-string for SO 50 and SO 100, the time scale is chosen in a far field from the pinch-off point.

I→V→IV was obtained for SO 50 and SO 100 due to the relatively larger viscous length and time scale [31]. Chen et al. [30] investigated the pinch-off of 83 % glycerol solution in air and the transition from I to IV regime was exhibited. In this work, the transition from I to IV regime through an intermediate V regime was demonstrated. Ohnesorge number for SO 50 is 0.55 and the transition route I→V→IV is in good agreement with the work of Castrejón-Pita et al. [13].

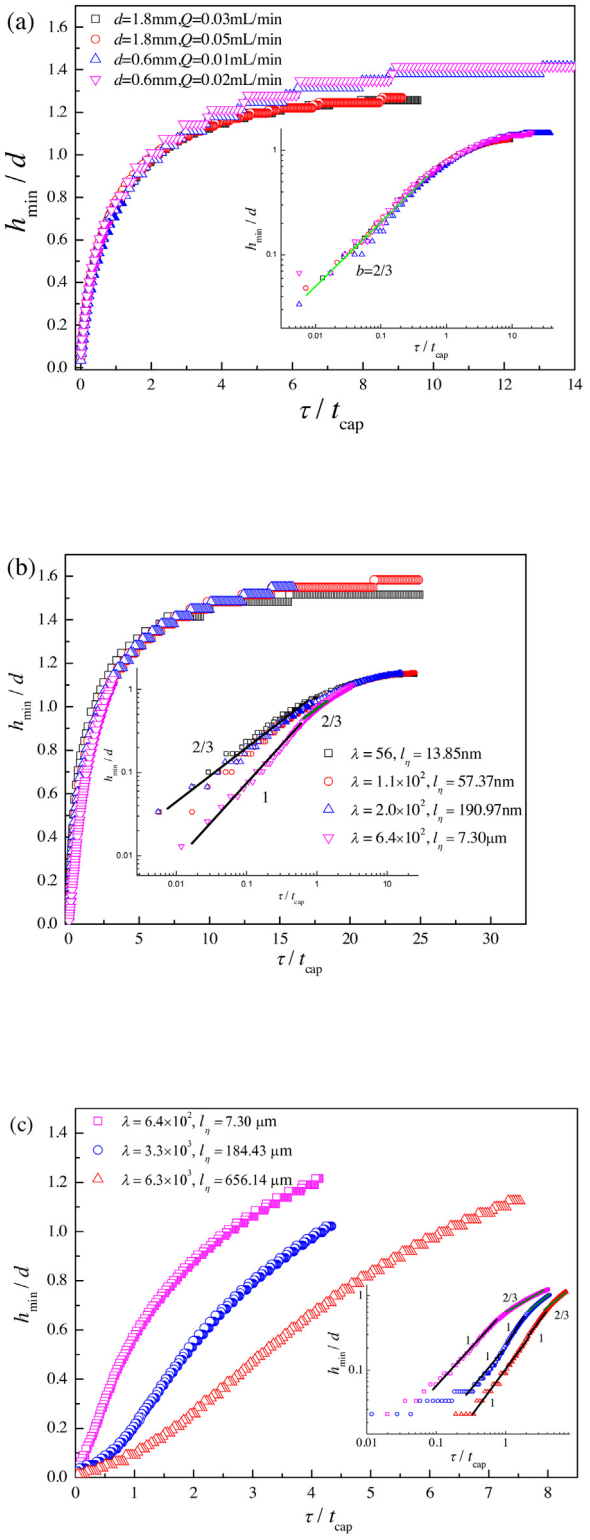

Fig. 4. Minimum neck diameter (h_{min}/d) as a function of time-to-pinch-off (τ/t_{cap}): (a) water with $\lambda = 56$, the exponent deviation is within 0.05; (b) relative low viscosity ratios, the exponent deviation is within 0.1; (c) silicone oils, the exponent deviation is within 0.1, Insets are the corresponding log-log plots.

Drop pinch-off in liquid-liquid two phase flow

Previous attentions are mainly dedicated to the drop pinch-off in air, and limited reports focused on the final pinch-off dynamics in viscous liquid. Fig. 5a and 5b shows liquid drops of various Newtonian fluids pinch off in SO 50 and SO 100, respectively. Compared to the drop pinch-off in air, the liquid thread evolution in viscous fluids is extremely different. In the pinch-off region, the bottom of the thread first starts to thin, followed by the upper end and then both ends thin simultaneously, resulting in a bulge in the middle. With temporary evolution, the bulge gathers together to be ellipsoidal while the two ends of the thread gradually thin to be a needle. Once pinching off from the two ends, the thread quickly detaches again from the bulge which finally develops into a spherical and large satellite drop. The disconnected thread undergoes interfacial instabilities and then evolves into cascades of sub-satellite drops. Such kind of cascade pinch-offs was highlighted in a numerical study [32], which shows the comparable shape evolution with our experiments. The large primary satellite droplet sandwiched by cascades of sub-satellite droplets up and down, leading to multiple instabilities. This differs from those of SO 50 and SO 100 pinch-off in air. On the one hand, the highly viscous external fluid exhibits a strong drag on the thread of internal fluid; on the other hand, the lower interfacial tension between two liquid phases compared to drop pinch-off in air enhances the surface instabilities and leads to multi-scale issues.

Particularly, during the pinch-off process, the fine thread at the upper end follows the motion of nozzle fluid and that at the bottom end follows the motion of the to-be-formed drop. The threads continuously stretch up and down, and after the final pinch-off, the two ends undergo several instabilities without instant rebound, which is quite different from the inviscid drop pinch-off in air. This is reasonably due to the fact that the strong viscous stress of the external fluid suppresses the thread's rebound after the release of surface tension [24,25]. In addition, for low-viscosity fluid pinch-off in air, the thread thins firstly at the bottom end and breaks there. However, the liquid thread of these fluids in viscous fluid thins at both ends and sometimes even breaks up first at the upper end. The stability of the liquid thread mainly depends on the importance of inertial, viscous force, and capillary force. When the inertial force is extremely larger than the capillary force, the pinch-off process switched from a "bottom breakup first" pattern to "upper breakup first" pattern [33]. In viscous fluid, the lower interfacial tension leads to a lower capillary force and the viscous stress from external fluid also takes a great effect, which enhances the instability of liquid thread in liquid-liquid two-phase system.

The viscosity ratio exerts a significant effect on the pinch-off behavior in viscous fluids. From Fig. 5a and 5b, the primary satellite droplet of $\lambda = 0.017$ is observed to be smaller than that of $\lambda = 0.061$. From Fig. 5c and 5d, the primary satellite droplet of $\lambda = 0.009$ is observed to be smaller than that of $\lambda = 0.032$. It needs to mention that though the interfacial tension affects the satellite drop size [23], the change of interfacial tension here varies in a negligible narrow range. Therefore, it could be concluded that the larger the viscosity ratio, the larger the primary satellite droplet. This can be explained that for a given external fluid, the larger viscosity of internal fluid tends to maintain the wholeness of the liquid thread, which leads to a larger primary satellite droplet. While for the given internal fluid, the larger viscosity of external fluid exerts a larger viscous stress and facilitates the satellite drop formation, which results in a smaller primary satellite droplet.

For the cascade of satellite drops, it was found that the number of satellite droplets changes with temporary evolution, the existing satellite drops grow but the primary satellite drop remains the same. It is very difficult to quantify the size distribution of satellite drops in the mode of beads-on-string due to the spatio-temporary instability, as well as the camera resolution. In addition, the upper liquid connected by the nozzle and the bottom liquid connected by the forming drop remains almost a stable cone shape when the liquid thread thins simultaneously up and down. The bottom cone shape gradually evolves into smooth surfaces instead of plane

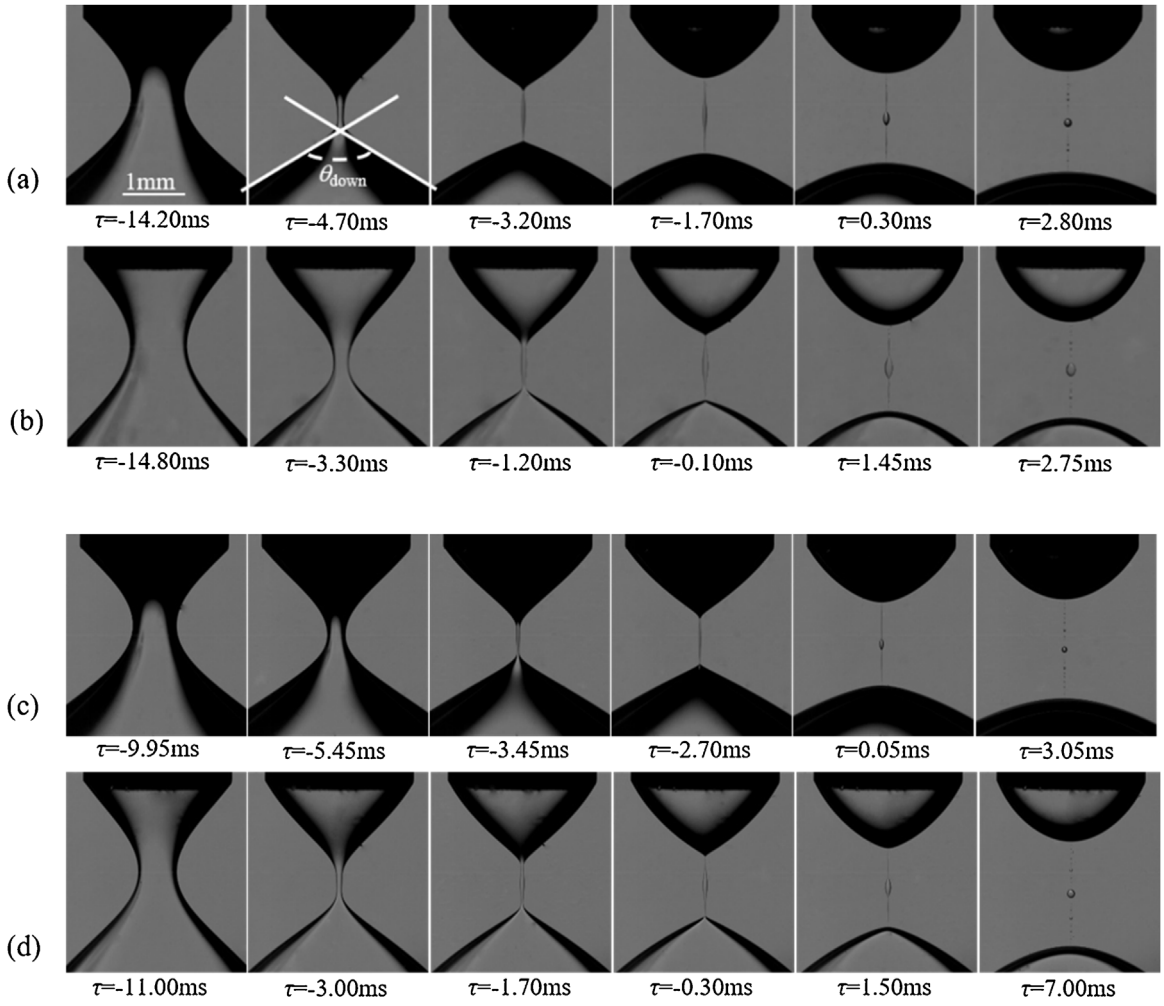

Fig. 5. Shape evolution of various aqueous drops pinching off in (a-b) SO 50 and (c-d) SO 100. (a) $\lambda = 0.017$; (b) $\lambda = 0.061$; (c) $\lambda = 0.009$; (d) $\lambda = 0.032$. All sequences in this figure share the same scaling bar.

surfaces, which is different from the self-similar pinch-off in air. The bottom cone angles θ_{down} shown in Fig. 5a were calculated and it was found that the viscosity of internal fluid exerts a more pronounced effect on the value of θ_{down}. For the same external fluid, the larger the viscosity of internal fluid, the smaller the value of θ_{down}. That is maybe due to the fact that the larger viscosity of internal fluid leads to the slow capillary pressure to pinch the liquid thread, which makes the liquid of the to-be-formed drop accumulates at the top and evolves into a small θ_{down} [29].

Fig. 6a and 6b show the profiles of liquid thread approaching to the pinch-off point under different viscosity ratios. Obviously, the profiles at relative larger time and length scales diverge from each other while the profiles at the local field around the pinch-off point are superimposed with each other, implying the persistence of self-similarity. This is in agreement with the work of Zhu and Wang [29], which demonstrated the thread profiles with $\lambda = 0.157$ and $\lambda = 0.039$, are superimposed onto a single form for three different times. Meanwhile, θ_{down} of $\lambda = 0.017$ in Fig. 6a is apparently larger than that of $\lambda = 0.061$ in Fig. 6b, which is the same with Fig. 5. The self-similar behavior was observed in our experiments with $0.009 \leq \lambda \leq 0.061$. Cohen et al. [19] once experimentally demonstrated that the self-similar behavior persists in the range of $0.02 \leq \lambda \leq 30$, and a good agreement is obtained by comparing the partly overlapped range of viscosity ratios with our experiments. Fig. 6c shows the profiles of liquid threads at $\lambda = 0.009$, $\lambda = 0.017$, $\lambda = 0.032$ and $\lambda = 0.061$. It was demonstrated that the profiles of liquid threads at different viscosity ratios are asymmetric and quickly evolve into a conic shape away from the minimum neck diameter h_{min}. The solid and open symbols in Fig. 6c indicate that the viscosity of external fluid enhances the profile difference between water and Emkarox solutions due to the increasing viscous stress of external fluid.

To confirm the observed thinning dynamics, we investigate the viscous two-fluid pinch-off behavior. Fig. 7 shows the dimensionless minimum neck diameter h_{min}/d as a function of dimensionless time-to-pinch-off τ/t_{cap} for drop pinch-off in SO 50 and SO 100. The flowrate in our experimental range shows a negligible effect on the evolution of minimum neck diameter even in the final pinch-off region, as shown in Fig. 7a. The nozzle diameter exhibits a large effect on the thread evolution in the initial stage. When the time approaches to the singularity point, the dimensionless neck diameter is basically overlapped in spite of some deviations due to the image resolution. Furthermore, Fig. 7b plots the neck evolution of drop pinch-off with different viscosity ratios. The thread evolution of drop pinch-off in SO 50 with $\lambda = 0.017$ and $\lambda = 0.061$ are almost the same. However, the thread evolution of drop pinch-off in SO 100 with $\lambda = 0.009$ and $\lambda = 0.032$ exhibits a big difference. By analyzing the rest tests, we further found that the external fluid enhances the effect of internal fluids on the pinch-off dynamics, which was also demonstrated in the above discussion of the thread profile. Therefore, the interaction between internal and external fluids is of significant importance for drop pinch-off in

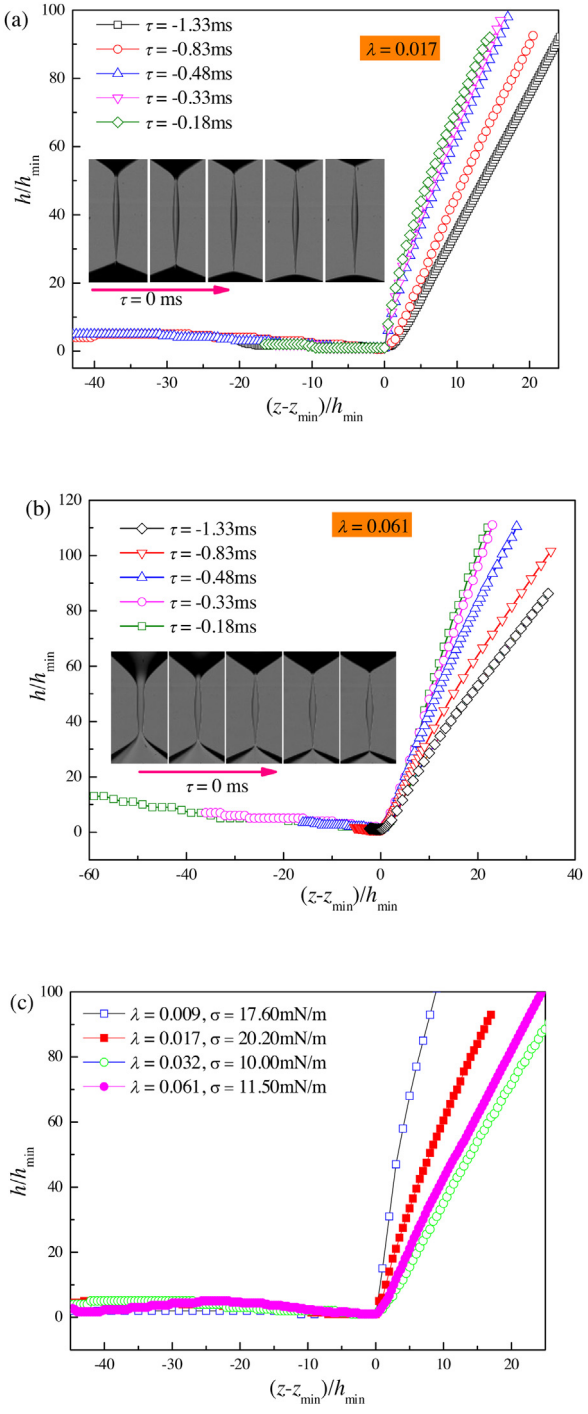

Fig. 6. Profiles of liquid thread in the very vicinity of first pinch-off point. (a) water pinch-off in SO 50 with λ = 0.017; (b) 4.50 wt% Emkarox aqueous drop pinch-off in SO 50 with λ = 0.061; (c) drop pinch-off with different viscosity ratios at τ = -0.48 ms, the solid symbol represents the pinch-off behavior in SO 50 and the open symbol stands for the pinch-off behavior in SO 100.

viscous fluids. Similarly, the power-law scaling was applied to investigate the drop pinch-off in viscous fluids and I→V transition was observed for all viscosity ratios. Castrejón-Pita et al. [13] once conducted the simulation of $Oh = 0.07$, and the results show the route of I→V→IV transition. In our work, Ohnesorge number for drop pinch-off in viscous fluids was much smaller than 1, the inertial regime (I) was followed by the viscous regime (V) and the inertial-viscous regime (IV) was unable to be detected because of the smaller viscous length scale out of optical resolution.

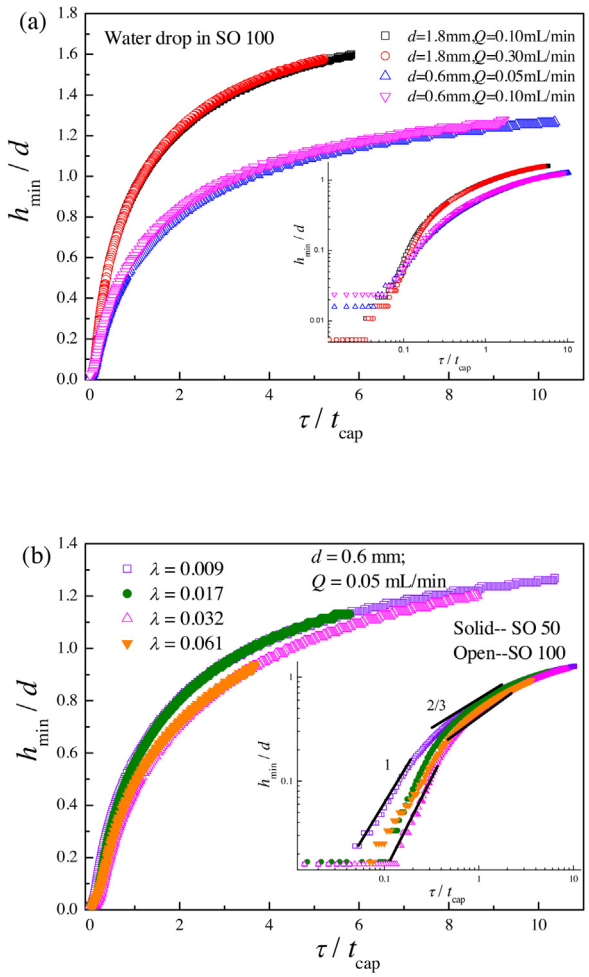

Fig. 7. (a)Minimum neck diameter (h_{min}/d) as a function of time-to-pinch-off (τ/t_{cap}) for water drop pinch-off in SO 100; (b) Minimum neck diameter (h_{min}/d) as a function of time-to-pinch-off (τ/t_{cap}) for drop pinch-off with different viscosity ratios.

Conclusion

In this paper, an experimental investigation was performed on the drop pinch-off mechanisms in air and viscous fluids. The results show the viscosity ratio strongly affects the drop pinch-off process as well as the profile and deformation. Within the investigated range of viscosity ratios, the self-similar profiles were observed as the time approached to the singularity point. For drop-in-air system, the final pinch-off stages were revealed in the inertial regime (I) for $\lambda = 1.1 \times 10^2$, $\lambda = 1.1 \times 10^2$ and $\lambda = 2.0 \times 10^2$; I→V transition was observed for $\lambda = 6.4 \times 10^2$; and I→V→IV transition took place for $\lambda = 3.3 \times 10^3$ and 6.3×10^3. For drop-in-liquid system, the route of I→V transition was obtained. These results were in good agreement with the experiments or simulations in the literature [13,23]. As the viscosity ratio was varied, the shape of the thread, satellite drop and newly formed drops differed [27]. Too large or too small viscosity ratios could amplify the instabilities of liquid thread and leads to multi-satellite droplets. Further works are still required to elucidate the role of combined viscous and elastic properties on the pinch-off process in the viscoelastic fluids. Interfacial instability could also be an interesting avenue to explore in liquid-liquid systems displaying low interfacial tension.

Declaration of Competing Interest

The authors report no declarations of interest.

Acknowledgement

This work is supported by the Fundamental Research Funds for the Central Universities (2019QNA09).

References

[1] R. Valette, E. Hachem, M. Khalloufi, A.S. Pereira, M.R. Mackley, S.A. Butler, J. Non-Newton. Fluid Mech. 263 (2019) 130.
[2] X.F. Jiang, Y.N. Wu, Y.G. Ma, H.Z. Li, Chem. Eng. Res. Des. 115 (2016) 262.
[3] G. Giménez-Ribes, L.M.C. Sagis, M. Habibi, Food Hydrocoll. 103 (2020)105616.
[4] R. Ma, T.T. Fu, Q.D. Zhang, C.Y. Zhu, Y.G. Ma, H.Z. Li, J. Ind. Eng. Chem. 54 (2017) 408.
[5] P. Zhu, T. Kong, L. Lei, X. Tian, Z. Kang, L. Wang, Sci. Rep. 6 (2016) 21527.
[6] T. Cubaud, B.M. Jose, S. Darvishi, R. Sun, Int. J. Multi. Flow 39 (2012) 29.
[7] J.B. Keller, M.J. Miksis, SIAM J. Appl. Math. 43 (1983) 268.
[8] D.H. Peregrine, G. Shoker, A. Symon, J. Fluid Mech. 212 (1990) 25.
[9] R.F. Day, E.J. Hinch, J.R. Lister, Phys. Rev.Lett. 80 (1998) 704.
[10] Y.J. Chen, P.H. Steen, J. Fluid Mech. 341 (1997) 245.
[11] D.M. Henderson, W.G. Pritchard, L.B. Smolka, Phy. Fluids 9 (1997) 3188.
[12] J. Dinic, L.N. Jimenez, V. Sharma, Lab A Chip. 17 (2017) 460.
[13] J.R. Castrejón-Pita, A.A. Castrejón-Pita, S.S. Thete, K. Sambath, I.M. Hutchings, J. Hinch, J.R. Lister, O.A. Basaran, Proc. Nat. Acad. Sci. 112 (15) (2015) 4582.
[14] A.U. Chen, P.K. Notz, O.A. Basaran, Phys. Rev. Lett 88 (2002)174501.
[15] Y. Li, J.E. Sprittles, J. Fluid Mech. 797 (2016) 29.
[16] P. Doshi, I. Cohen, W.W. Zhang, M. Siegel, P. Howell, O.A. Basaran, Science 302 (2003) 1185.
[17] J.R. Lister, H.A. Stone, Phys. Fluids 10 (1998) 2758.
[18] Y. Pan, K. Suga, J. Fluids Eng. 125 (2003) 922.
[19] I. Cohen, M.P. Brenner, J. Eggers, S.R. Nagel, Phys. Rev. Lett. 83 (1999) 1147.
[20] W.W. Zhang, J.R. Lister, Phys. Rev. Lett. 83 (6) (1999) 1151.
[21] X.F. Jiang, C.Y. Zhu, Y.G. Ma, H.Z. Li, Adv. Mater. Interf. 4 (2017)1700193.
[22] N. Dietrich, S. Poncin, H.Z. Li, Exp. Fluids 50 (2011) 1293.
[23] N.M. Kovalchuk, H. Jenkinson, R. Miller, M.J.H. Simmons, J. Coll. Interf. Sci. 516 (2018) 182.
[24] P. Dastyar, M.S. Salehi, B. Firoozabadi, H. Afshin, J. Ind. Eng. Chem. 89 (2020) 183.
[25] J. Eggers, Rev. Mod. Phys. 69 (3) (1997) 865.
[26] L.B. Smolka, A. Belmonte, J. Non Newton. Fluid Mech. 115 (1) (2003) 1.
[27] X.D. Shi, M.P. Brenner, S.R. Nagel, Science 265 (1994) 219.
[28] J.C. Burton, P. Taborek, Phys. Rev. Lett. 101 (2008)214502.
[29] P. Zhu, L. Wang, Chem. Eng. Sci. 196 (2019) 333.
[30] A.U. Chen, P.K. Notz, O.A. Basaran, Phys. Rev. Lett. 88 (17) (2002)174501.
[31] J. Eggers, Phys. Rev. Lett. 71 (21) (1993) 3458.
[32] J.C. Burton, P. Taborek, Phys. Rev. Lett. 98 (2007)224502.
[33] Y.C. Liao, H.J. Subramani, E.I. Franses, O.A. Basaran, Langmuir 20 (23) (2004) 9926.